Supporting Information

Technical note: On the selection of precooling loops for low-temperature continuous flow chemistry.

James A. K. Cochrane[a] and Raminder S. Mulla[a]*[+]

a) Sygnature Discovery Ltd., BioCity, Pennyfoot St., Nottingham NG1 1GR, UK

*Corresponding author. Email: raminder@ctsci.co.uk

Table of Contents

1 Experimental....2
1.1 Materials and general remarks....2
1.2 Analysis....2
1.3 Precooling characterisation studies....3
1.3.1 Effect of bath temperature on ΔT....3
1.3.2 Thermocouple error estimation at low temperature....3
1.3.3 Definition of the cooling bath: Impact of agitation....4
1.3.4 Effect of solvent on cooling bath efficacy....5
1.3.5 Estimation of errors in residence time....5
1.4 Synthetic Procedures....6
1.4.1 Flow procedure for lithiation-formylation of 4-Bromo-3-fluoroanisole, **1**....6
1.4.2 Flow procedure for lithiation-protonation of 1,2-Dibromobenzene, **3**....6
2 Additional information....7
2.1 Derivation of a simple precooling model....7
2.2 Validation of the model....9
2.2.1 Introductory notes....9
2.2.2 Simulated residence time -ΔT profiles....9
2.2.3 Comparison of calculated and experimental values....10
2.3 Reference Chromatograms....11
2.3.1 Lithiation-formylation of 4-Bromo-3-fluoroanisole, **1**....11
2.3.2 Chromatograms supporting yield calculations for table 3....11
2.3.3 Calibration curve for yield determination of aldehyde **2**....12
2.4 Lithiation-protonation of 1,2-Dibromobenzene, **3**....13
2.4.1 Chromatograms supporting yield calculations for table 4....13
2.4.2 Calibration curve for yield determination of **4**....14
2.5 T_{react}-Yield correlations....14
2.6 Equipment photos....15
2.6.1 Effect of residence time on Δ T....15
2.6.2 Application to cryogenic flow chemistry: Scope and limitations....16
3 Source literature for Figure 1....18

Downloaded from pubs.acs.org/oprdfk/article-supplement/5455873/pdf/op6c00246_si_002/ by guest on 23 October 2026

+ Present address: Coretech Sciences Ltd., Liverpool Science Park, 131 Mount Pleasant, Liverpool, L3 5TF, U.K.

1 Experimental

1.1 Materials and general remarks.

Methyl 3,5-dinitrobenzoate (TraceCERT grade, CAS No: 2702-58-1) was purchased from Aldrich and used as received as qNMR standard. 4-Bromo-3-fluoroanisole **1** (CAS No: 458-50-4) was purchased from BLD GmbH and used as received at 100±2 % qNMR purity. 2-Fluoro-4-methoxybenzaldehyde **2** (CAS No: 331-64-6) was purchased from Fluorochem and used as received at 94±2 % qNMR purity.

1,2-Dibromobenzene **3** (CAS No: 583-53-9) was purchased from Apollo Scientific and used as received at 100±2 % qNMR purity. Bromobenzene **4** (CAS No: 108-86-1) was purchased from Aldrich and used as received at 100±2 % qNMR purity.

n-HexLi (CAS No: 21369-64-2) (2.3M in hexane) was purchased from Aldrich and used as received. 1.5M n-HexLi was prepared by dilution with dry heptane (purchased from Aldrich). Anhydrous DMF (CAS No: 68-12-2) was purchased from Thermo Fisher Scientific and was also used as received. Anhydrous THF was purchased from Thermo Fisher and used as received. 2-MeTHF was also purchased from the same source and used as received.

Syringe pumps were New Era model NE-1000 syringe pumps purchased from WPI Europe and were controlled using the Syringe Pump Pro software (https://syringepumppro.com/). MR-QD syringe pumps were purchased from LTF GmbH. PTFE tubing and 1/4-28 UNF fluidic connections were sourced from Bohlender GmbH. PFA tubing was sourced from Uniqsis or ESSKA. 316 stainless steel tubing was purchased from Swagelok and Amazon UK. Tee pieces (Ø = 500 µm) were manufactured by Bohlender GmbH (cat. no. F707-14) and purchased through Labtex UK . Tee pieces of (Ø = 250 µm) were manufactured by VICI (cat. no. CTCKF) and purchased through Thames Restek . Exposed-end K-type thermocouples (cat. no. TWSSTK00002M00P1) were purchased from Sterling Sensors. The datalogger used was a Lascar EL-GFX-DTC ordered from RS electronics, UK.

All reactors were primed with at least 3 volumes of dry THF prior to each experiment to ensure air and moisture-free operating conditions. Cooling baths were agitated at a speed sufficient to form a vortex in the cooling fluid, either via stir bar or overhead stirrer.

1.2 Analysis

LCMS analyses were performed using a Waters Cortecs C18, 2.7 µm, 30x2.1 mm column at 40 °C, 1 minute method, 0.1 % Formic acid, 2-100 % MeCN/water coupled to an Agilent mass spectrometer. NMR spectra were recorded using a Bruker 400 MHz Avance Neo spectrometer fitted with a Bruker 5 mm iProbe, or a Bruker 500 MHz Avance III HD spectrometer equipped with a Bruker 5 mm SmartProbeTM. Spectra were measured at 298 K, unless indicated otherwise. Data were acquired using Bruker TopSpin software. All data (LCMS and NMR) were processed using MestreNova software.

Downloaded from pubs.acs.org/oprdfk/article-supplement/5455873/pdf/op6c00246_si_002/ by guest on 23 October 2026

1.3 Precooling characterisation studies.

1.3.1 Effect of bath temperature on ΔT.

THF was pumped through the setup depicted in **Figure 2** of the main text with ID x OD = 1 x 1.6 mm PFA tubing at a flow rate of 6.6 mL/min and a residence time of 10 s, while allowing the stirred cooling bath to slowly warm from -55 °C to 0 °C. Inline and bath temperatures were continuously recorded using K-type thermocouples. The invariance of ΔT across a range of temperatures is demonstrated in Figure S1. A preliminary run with extended low temperature range (-80 °C to 0°C) was also performed.

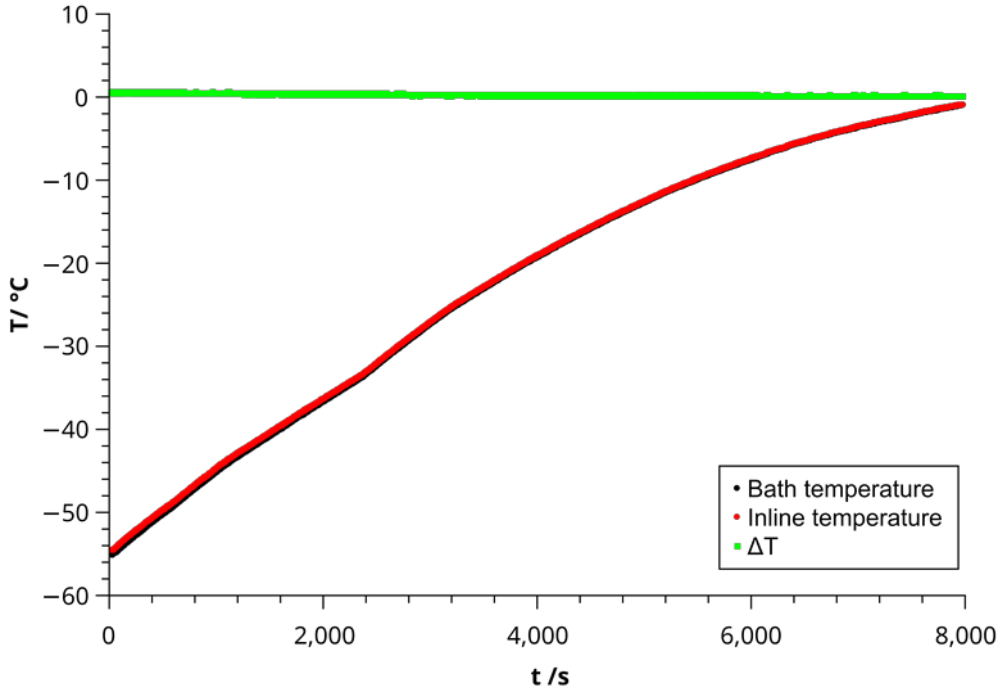


Figure S1: Variation of the absolute difference between bath and inline temperature, ΔT over the course of a temperature ramp experiment.

1.3.2 Thermocouple error estimation at low temperature.

A Pt100 probe and two K-type thermocouples were immersed in a stirred dry ice -acetone bath at -60 °C and readings were allowed to stabilise. Errors were estimated via an error propagation approach in which the reading from the Pt100 probe was treated as a reference value as below:

$$\frac{\delta T}{T} = \sqrt{\left(\frac{\delta T_k}{T_{Pt100}}\right)^2}$$

Where: δT is the estimated error, T is the K-type thermocouple reading, δT_k is the standard deviation between the averaged K-type thermocouple readings and T_{Pt100} is the bath temperature according to the reading from the Pt100 probe.

In this approach, T_{Pt100} is treated as the “true” temperature and δT/T values were of an average value of 0.973 ± 0.004, meaning the estimated error in T was ±3 % of the absolute value of T. Across the temperature ranges studied, this translated to a temperature dependent error of ± 2 °C, which was conservatively rounded to ± 2.5 °C for reporting purposes.

Downloaded from pubs.acs.org/oprd/fk/article-supplement/5455873/pdf/op6c00246_si_002/ by guest on 23 October 2026

1.3.3 Definition of the cooling bath: Impact of agitation

Following the approach depicted in **Figure 2** of the main text, PFA tubing (ID = 1 mm, OD = 1.6 mm, L 108 cm) was attached to an inline thermocouple and immersed in a static iPrOH/dry ice bath equipped with 3 thermocouples in different positions of the bath. THF was then pumped through the tubing across a range of flow rates (2.5 to 48 mL/min) giving a range of residence time of 1.05 to 20 s. Once readings from all thermocouples stabilised, temperatures were recorded.

The average bath temperature from the three immersed thermocouples was calculated and used to generate a ΔT value ($\Delta T = |T_{bath}-T_{inline}|$) for each residence time point, which was then plotted against R_t using either: the averaged thermocouple reading as T_{bath} , or individual thermocouple readings. When the bath was agitated via overhead stirring, any difference in ΔT arising from thermocouple positioning was eliminated and lower ΔT values were observed (Figure S2). Mean Euclidean distances taken between the average ΔT and ΔT_1, ΔT_2, and ΔT_3 at constant R_t serve as a metric for cooling bath homogeneity. In the unstirred case this was 1.8 while in the stirred case the distance was 0.8, the lower value indicating better homogeneity.

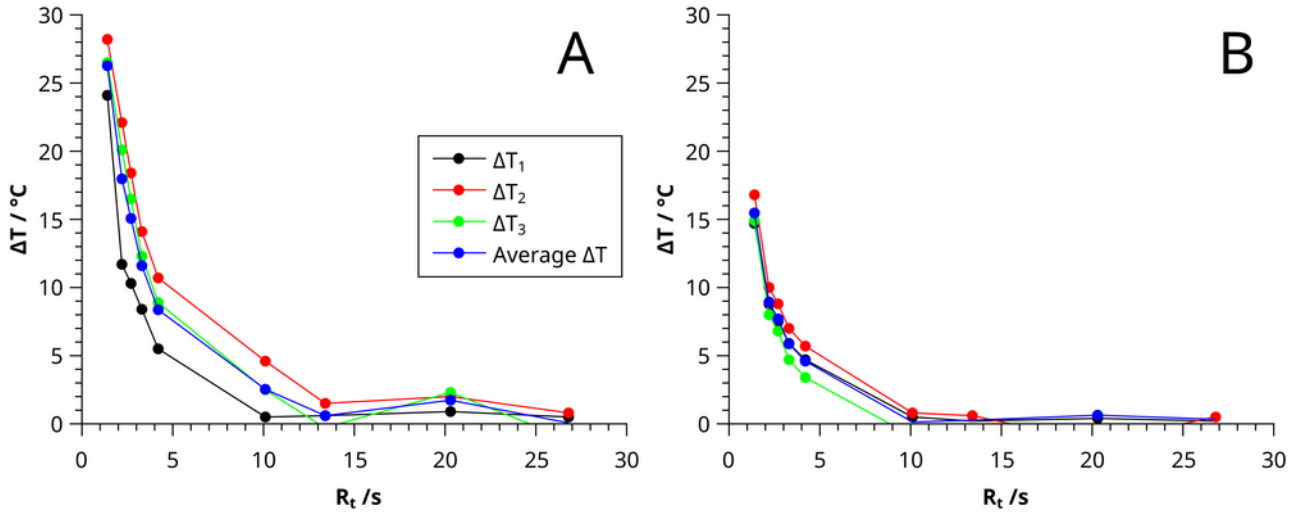


Figure S2: ΔT as a function of residence time in: A) an unstirred dry ice/iPrOH bath and B) a stirred dry ice/iPrOH bath. ΔT_1, ΔT_2, and ΔT_3 curves are plotted using localised T_{bath} values measured from different thermocouple positions in the bath. Average ΔT is plotted using the average of those measured, localised, T_{bath} values.

Downloaded from pubs.acs.org/oprd/fk/article-supplement/5455873/pdf/op6c00246_si_002/ by guest on 23 October 2026

1.3.4 Effect of solvent on cooling bath efficacy.

Dry ice baths using different solvents (acetone, MeOH) were then compared using the R_t required for minimisation in ΔT as the metric for selection. Based on these data, agitated dry ice baths using both acetone and MeOH are superior to iPrOH baths (Figure S3), with acetone being chosen as solvent on a cost and toxicity basis.

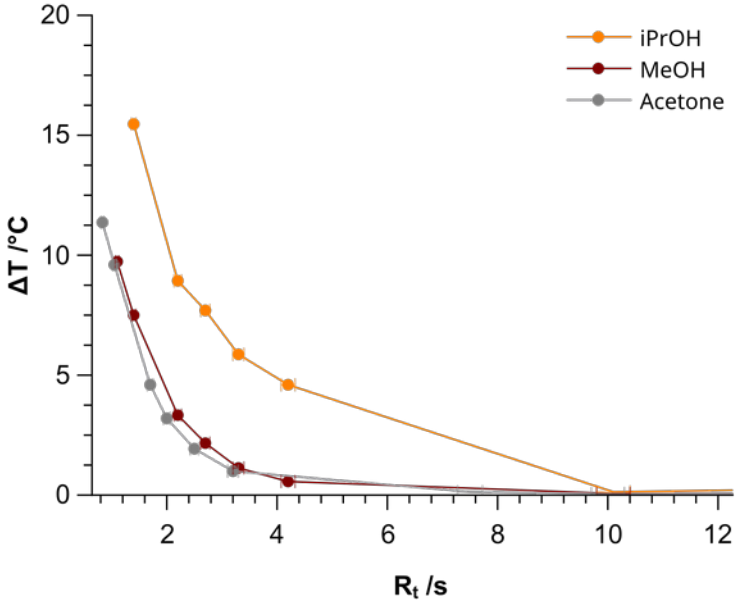


Figure S3: Effect of cooling bath composition on ΔT.

1.3.5 Estimation of errors in residence time.

The error propagation expression used was that for a quotient, since:

$$R_t = \frac{V}{Q} \text{ therefore}$$

$$\frac{\delta R_t}{R_t} = \sqrt{\left(\frac{\delta Q}{Q}\right)^2 + \left(\frac{\delta V}{V}\right)^2}$$

The error in tube volume, δV, was assessed via dye elution studies in which the tubing under study was assumed to be a perfect cylinder of:

$$V = \frac{\pi D^2 h}{4}$$

Where all symbols have their usual meanings. The error in flow rate, δQ, was evaluated through the setting of a flow rate, Q, at the pump to pump a volume of water over 1 minute into a pre-tared vial. The vial was then weighed and the difference between the expected and measured mass of water (assuming a density of 1 g cm^{-3}) was then treated as δQ. A typical error ratio, $\delta R_t/R_t$ was calculated to be 3.2%.

Downloaded from pubs.acs.org/oprd/fk/article-supplement/5455873/pdf/op6c00246_si_002/ by guest on 23 October 2026

1.4 Synthetic Procedures

A note on safety: n-HexLi is flammable and pyrophoric. Only suitably trained, experienced personnel should operate the processes described. Many reactions involving arynes are also at risk of thermal runaway, and so appropriate risk assessments and corrective action plans must be put in place prior to execution.

1.4.1 Flow procedure for lithiation-formylation of 4-Bromo-3-fluoroanisole, 1.

For runs at 0.3 M: Following the reactor configuration in **Figure 7** of the main text were mixed **1** (0.3 M in THF) delivered at 17 mL/min and hexyllithium (2.3M, 1.10 eq. in hexane) delivered at 2.45 mL/min in a 0.5 mm T-piece at the bath temperature set-point, T_{bath}. The stream was held in residence for 1 s and then mixed with DMF (1 M in THF, 1.20 eq) delivered at 6.12 mL/min in a second 0.5 mm T-piece also at T_{bath}. The stream was held in residence for 2 s before collection into MeOH. Collection began at steady state after infusing 3 residence times of all feed solutions through the reactor. qLC yields of **2** were calculated based on 60 s of steady state collection.

For runs at 0.5 M: Following the reactor configuration in **Figure 7** of the main text were mixed **1** (0.5 M in THF) delivered at 17 mL/min and hexyllithium (2.3M, 1.10 eq. in hexane) delivered at 4.05 mL/min in a 0.5 mm T-piece at the bath temperature set-point, T_{bath}. The stream was held in residence for 1 s and then mixed with DMF (1.6 M in THF, 1.20 eq) delivered at 6.35 mL/min in a second 0.5 mm T-piece also at T_{bath}. The stream was held in residence for 2 s before collection into MeOH. Collection began at steady state after infusing 3 residence times of all feed solutions through the reactor. qLC yields of **2** were calculated based on 60 s of steady state collection.

1.4.2 Flow procedure for lithiation-protonation of 1,2-Dibromobenzene, 3

Following the reactor configuration in **Figure 8** of the main text were mixed bromoarene **3** (0.27 M in THF) delivered at 6 mL/min and hexyllithium (1.5M, 1.10 eq. in hexane) delivered at 1.2 mL/min in a 0.25 mm T-piece at the bath temperature set-point, T_{bath}. The stream was held in residence for 0.8 s and then mixed with neat MeOH (24.7 M, 91 eq) delivered at 6 mL/min in a 0.5 mm T-piece also at T_{bath}. The stream was held in residence for 1.8 s before collection into MeOH. Collection began at steady state after infusing 3 residence times of all feed solutions through the reactor. qLC yields of **4** were calculated based on 60 s of steady state collection.

Downloaded from pubs.acs.org/oprdfk/article-supplement/5455873/pdf/op6c00246_si_002/ by guest on 23 October 2026

2 Additional information

2.1 Derivation of a simple precooling model

Assume that a precooling line is a perfect cylinder whose surface area A_S is given by:

$$A_s = 2\pi r(r+l) \text{ and } D = 2r$$

Where D is diameter, r is radius and l is length, so:

$$A_s = \pi D\left(\frac{D}{2}+l\right)$$

Expressing line length as a function of the residence time R_t: given $l = V R_t$ because distance travelled in a pipe relates to linear flowrate, i.e. volumetric flow rate Q over cross sectional area A_c. Then:

$$V = \frac{Q}{A_c} = \frac{Q}{\pi r^2} = \frac{4Q}{\pi D^2}$$

l can be written as:

$$l = \frac{4QR_t}{\pi D^2}$$

Substituting into the area relation and simplifying:

$$A_S = \frac{\pi D^2}{2} + \frac{4QR_t}{D} = \frac{\pi D^3}{2D} + \frac{8QR_t}{2D}$$

$$A_s = \frac{1}{2D}\left(\pi D^3 + 8QR_t\right)$$

This expression for A_S will be used later.

The cooling equation for a pipe through which fluid flows in laminar flow, in a heat exchange medium at constant temperature is defined as:

$$T_{inline} = T_{bath} - \left(T_{bath} - T_{input}\right)\exp\left(-\frac{hA_s}{mC_p}\right)$$

Where: $T_{inline}, T_{bath}, T_{input}$ are the fluid temperatures on exiting the precooling line, the bath temperature and the temperature on entry into the precooling line respectively. h is the heat transfer coefficient m is the mass flow rate and $C_p$is the specific heat capacity. Taking natural logarithms:

$$T_{inline} - T_{bath} = -\left(T_{bath} - T_{input}\right)\exp\left(-\frac{hA_s}{mC_p}\right)$$

$$T_{bath} - T_{inline} = \left(T_{bath} - T_{input}\right)\exp\left(-\frac{hA_s}{mC_p}\right) \rightarrow \ln\left(\frac{T_{bath} - T_{inline}}{T_{bath} - T_{inline}}\right) = -\frac{hA_s}{mC_p}$$

Volumetric flow rate Q is a more practical unit to work in, relating to mass flow rate by $\rho = \frac{m}{Q}$, so:

$$\ln\left(\frac{T_{bath} - T_{inline}}{T_{bath} - T_{input}}\right) = -\frac{hA_s}{\rho QC_p}$$

Downloaded from pubs.acs.org/oprdfk/article-supplement/5455873/pdf/op6c00246_si_002/ by guest on 23 October 2026

The value for h, can be approximated by introducing the Nusselt number, $Nu=\frac{hD}{k}$, where D is the pipe diameter, and k the thermal conductivity. Substituting, we obtain:

$$\ln\left(\frac{T_{bath}-T_{inline}}{T_{bath}-T_{inline}}\right)=-\frac{Nu k A_s}{\rho Q C_p D}$$

To express the solvent dependence of the temperature differences more explicitly, we introduce the Prandtl number Pr, in its viscosity form:

$$Pr=\frac{C_p \mu}{k}$$

where μ is dynamic viscosity. Rearranging and substituting:

$$\ln\left(\frac{T_{bath}-T_{inline}}{T_{bath}-T_{inline}}\right)=-\frac{Nu C_p \mu A_s}{Pr \rho Q C_p D}=-\frac{Nu \mu A_s}{Pr \rho Q D}$$

Introduce the surface area A_S as a function of residence time. Let:

$$-\frac{Nu \mu}{Pr \rho Q D}=-\frac{S}{D}$$

Where S is a grouped, solvent-dependent parameter. Then:

$$\ln\left(\frac{T_{bath}-T_{inline}}{T_{bath}-T_{input}}\right)=-\frac{Nu \mu}{Pr \rho Q D}\left(\frac{1}{2D}\left(\pi D^3+8 Q R_t\right)\right)\rightarrow-\frac{S}{D}\left(\frac{1}{2D}\left(\pi D^3+8 Q R_t\right)\right)$$

Which can be expressed as:

$$\ln\left(\frac{T_{bath}-T_{inline}}{T_{bath}-T_{input}}\right)=\frac{-S\pi D^3-S8 Q R_t}{2D^2}$$

Which can alternatively be written as:

$$\ln\left(\frac{T_{bath}-T_{inline}}{T_{bath}-T_{input}}\right)=-S\left(\frac{\pi D}{2}+\frac{4 Q R_t}{D^2}\right)$$

Reintroducing Pr and Nu:

$$\ln\left(\frac{T_{bath}-T_{inline}}{T_{bath}-T_{input}}\right)=\frac{-Nu \mu}{Pr \rho}\left(\frac{\pi D}{2Q}+\frac{4 R_t}{D^2}\right)$$

Let $\Delta T=|T_{bath}-T_{inline}|$. Taking the exponential:

$$\frac{\Delta T}{T_{bath}-T_{input}}=\left|\exp\left(\frac{-Nu \mu}{Pr \rho}\left(\frac{\pi D}{2Q}+\frac{4 R_t}{D^2}\right)\right)\right|$$

Which rearranges to:

$$\Delta T=\left|\left(T_{bath}-T_{input}\right)\exp\left(\frac{-Nu \mu}{Pr \rho}\left(\frac{\pi D}{2Q}+\frac{4 R_t}{D^2}\right)\right)\right|$$

Giving ***Equation 1*** in the main text[1].

1 The expression can be differentiated to find minima in the rate of change for ΔT. We opted not to use this approach in the main text to keep the comparison between experimental and calculated data as fair as possible.

Downloaded from pubs.acs.org/oprdfk/article-supplement/5455873/pdf/op6c00246_si_002/ by guest on 23 October 2026

2.2 Validation of the model

2.2.1 Introductory notes

Values for calculations are expressed below and were sourced from the literature.

T_{bath} / °C	-60
T_{input} /°C	22
Bulk mean temperature, T_{mean}/°C	-19
Modelled T_{mean} /°C	-23
μ (-23°C) /Pa s	0.000826
C_p (-23°C) /J kg^{-1} k^{-1}	1575
K (-23°C) /W m^{-1} k^{-1}	0.172
Pr /No units	7.564
ρ (-23°C)/ kg m^{-3}	933

Calculations were performed using LibreOffice Calc and a Python script, both of which are included in the raw data package for this work.

2.2.2 Simulated residence time -ΔT profiles

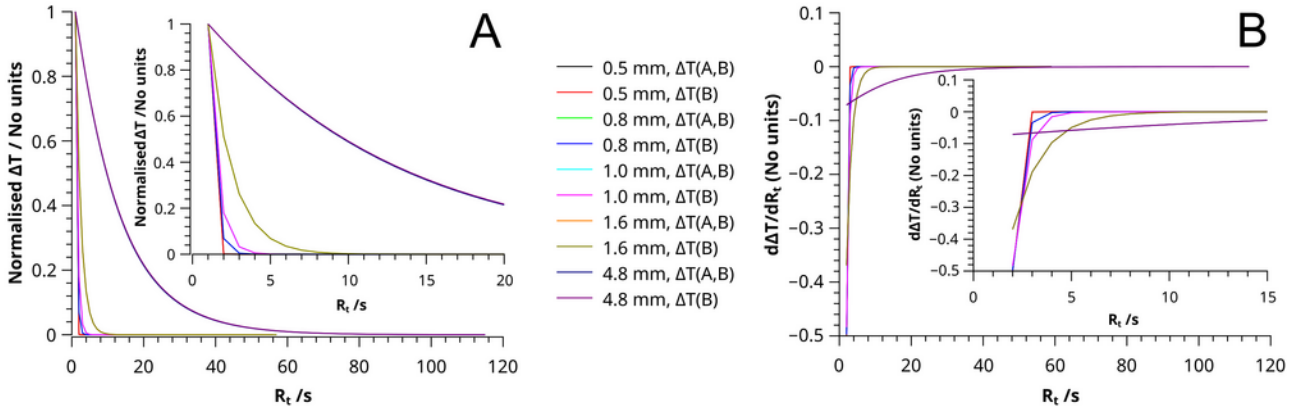


Figure S4: A) Curves generated using the derived precooling model, showing the effect of including and excluding the flow rate "A" term of equation 1 in the main text, termed as ΔT(A,B) and ΔT(B) respectively. B) The associated derivative curves.

Downloaded from pubs.acs.org/oprdfk/article-supplement/5455873/pdf/op6c00246_si_002/ by guest on 23 October 2026

2.2.3 Comparison of calculated and experimental values

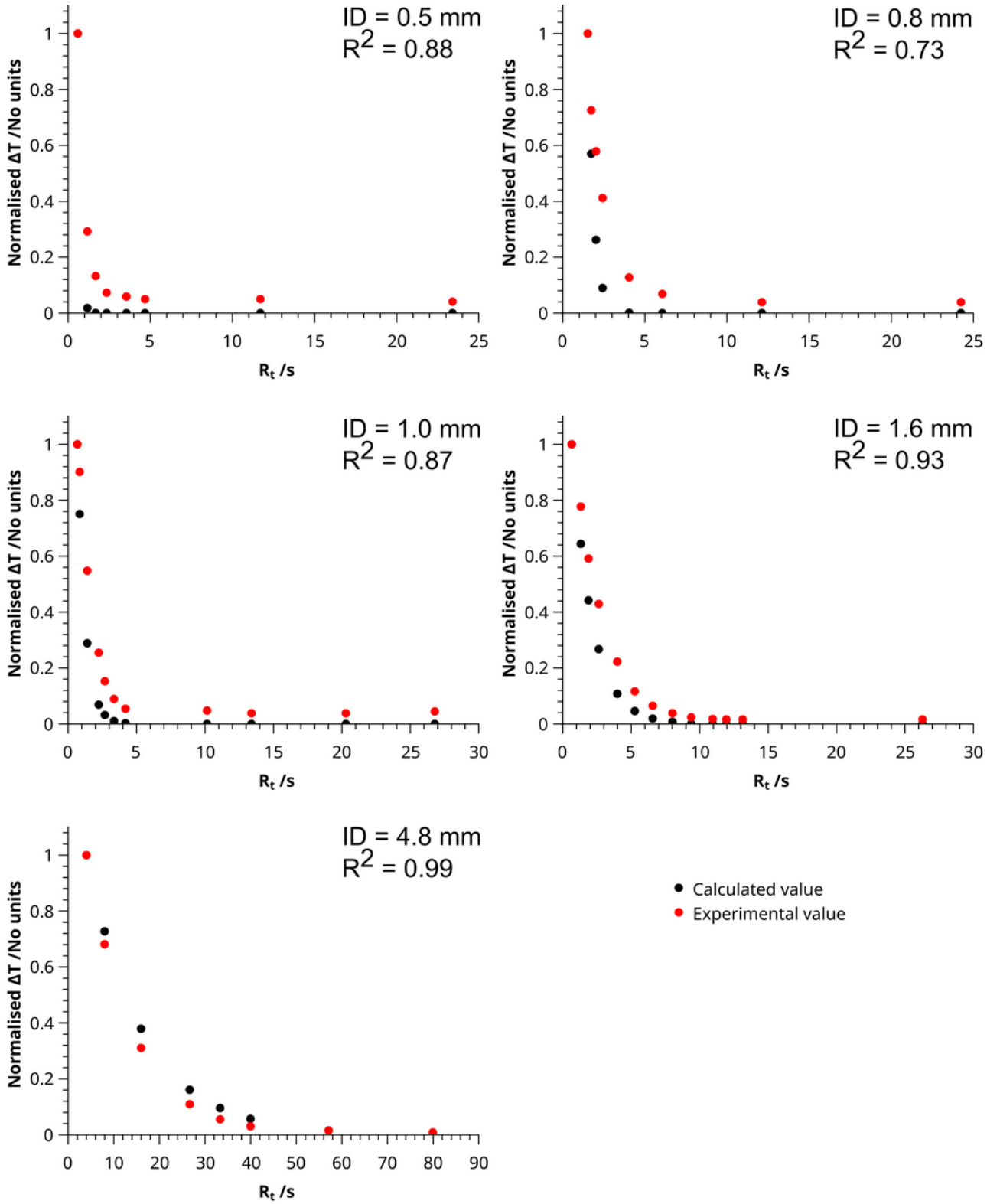


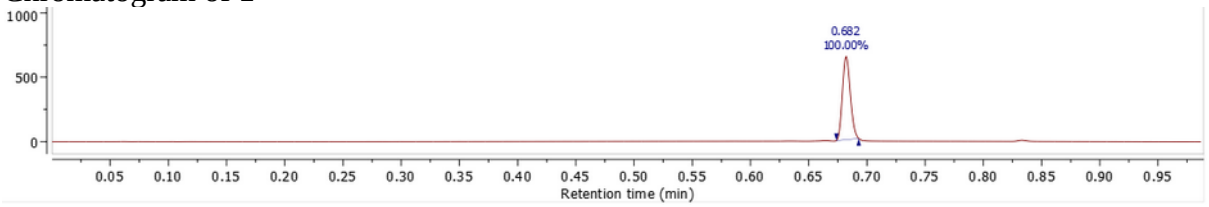
Figure S5: Comparison between calculated and experimental ΔT values. R^2 was calculated via the scikit-learn Python library.

Downloaded from pubs.acs.org/oprdfk/article-supplement/5455873/pdf/op6c00246_si_002/ by guest on 23 October 2026

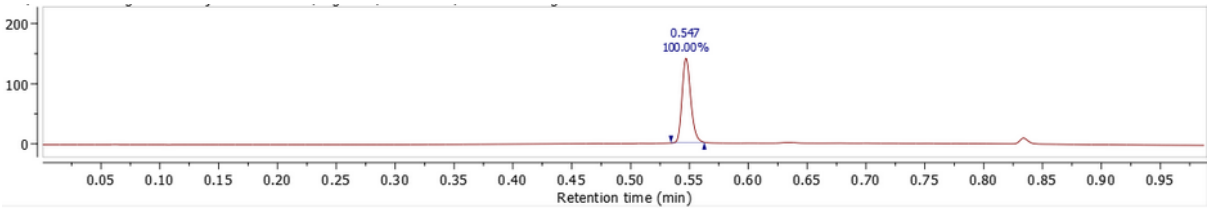
2.3 Reference Chromatograms

2.3.1 Lithiation-formylation of 4-Bromo-3-fluoroanisole, 1

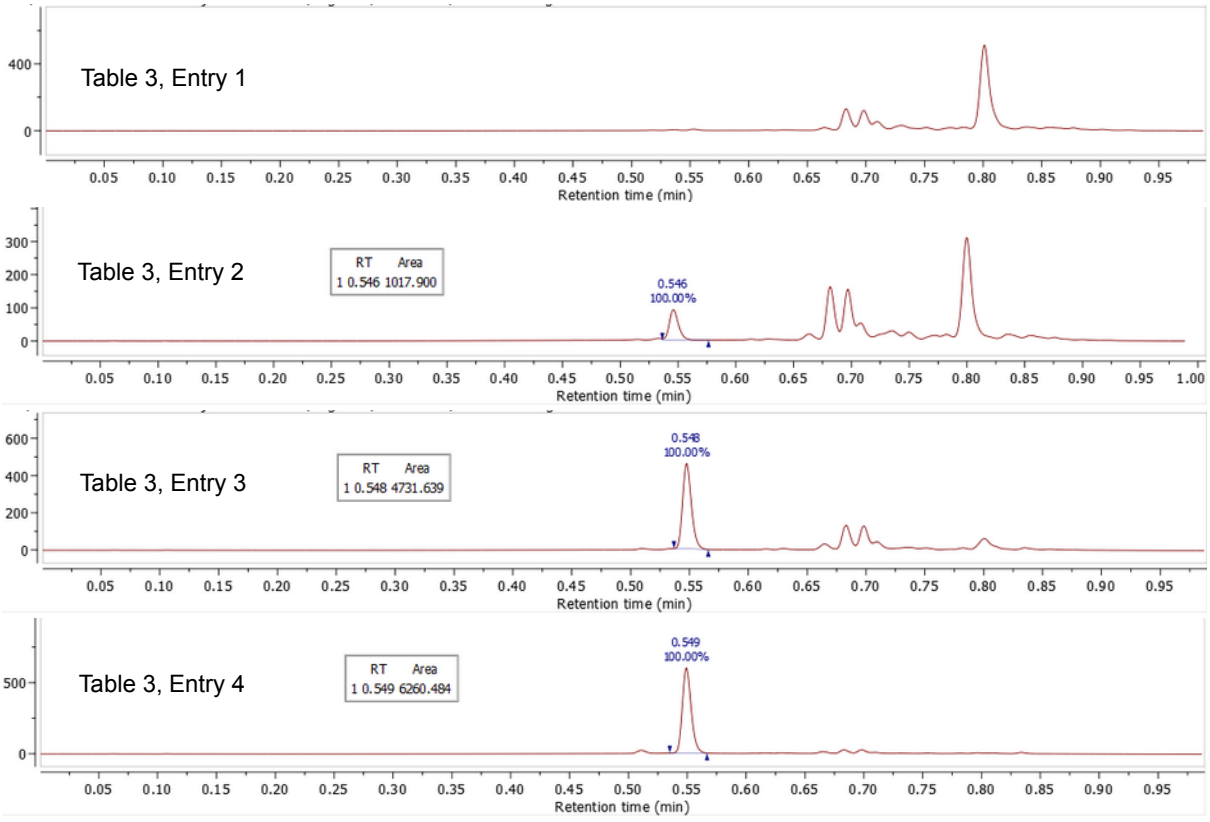
Chromatogram of **1**



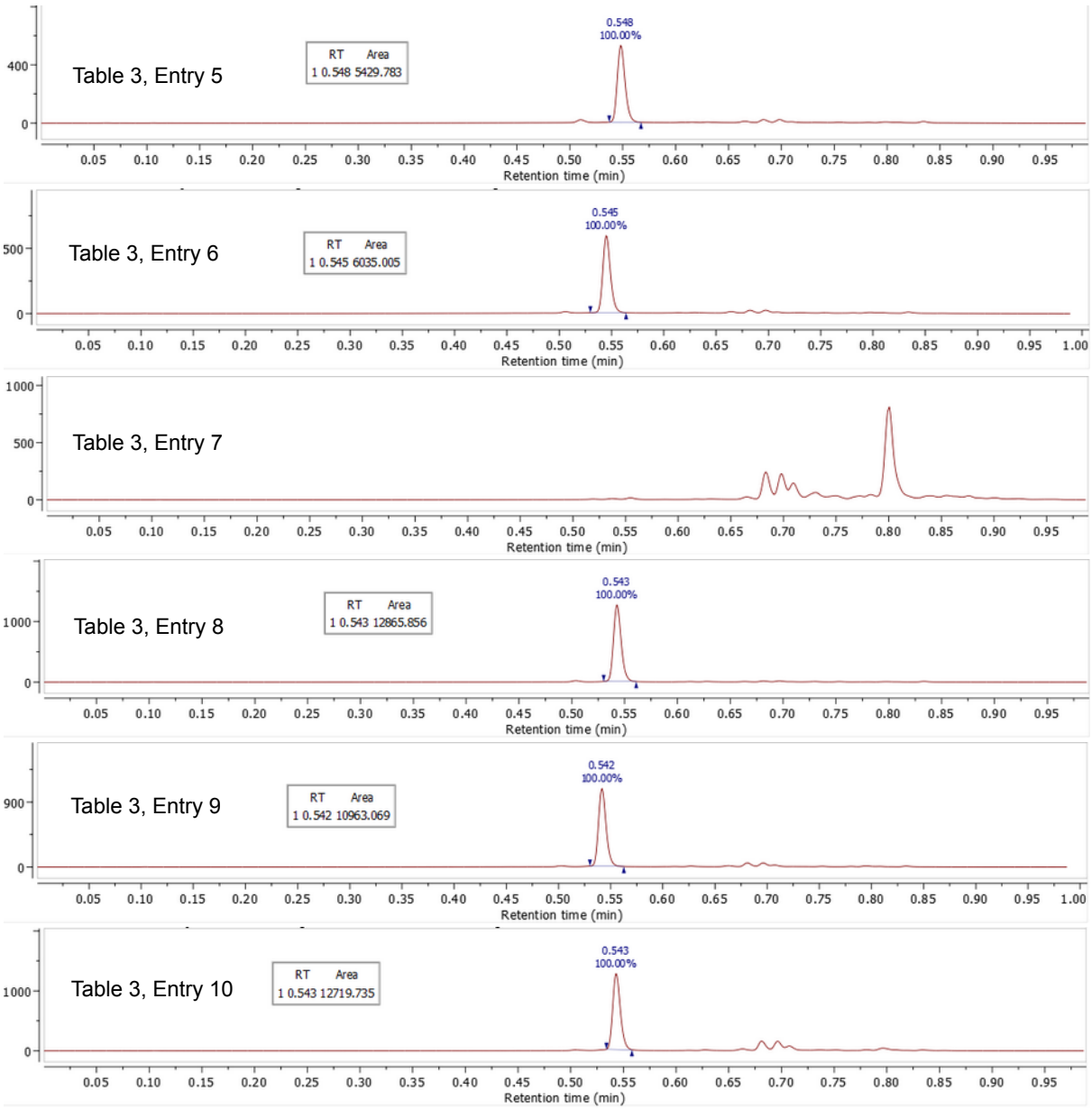
Chromatogram of **2**



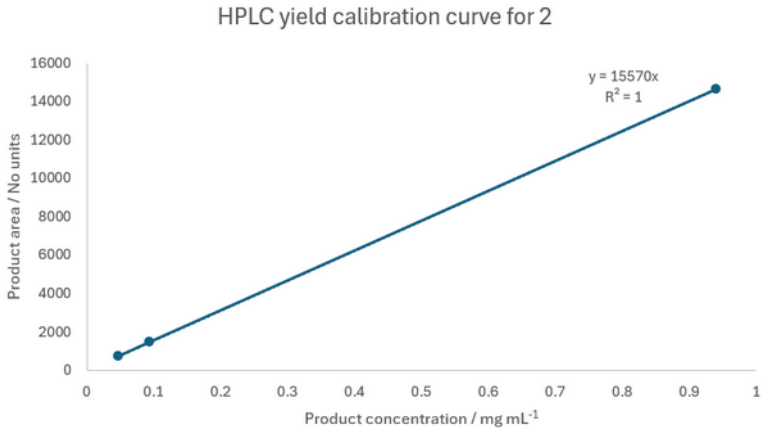
2.3.2 Chromatograms supporting yield calculations for table 3



Downloaded from pubs.acs.org/oprdfk/article-supplement/5455873/pdf/op6c00246_si_002/ by guest on 23 October 2026



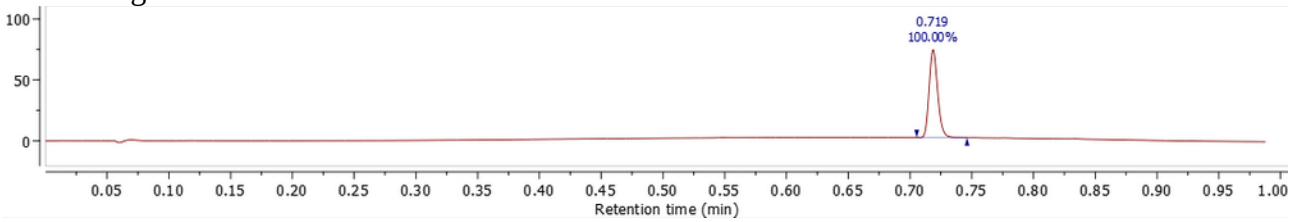
2.3.3 Calibration curve for yield determination of 2



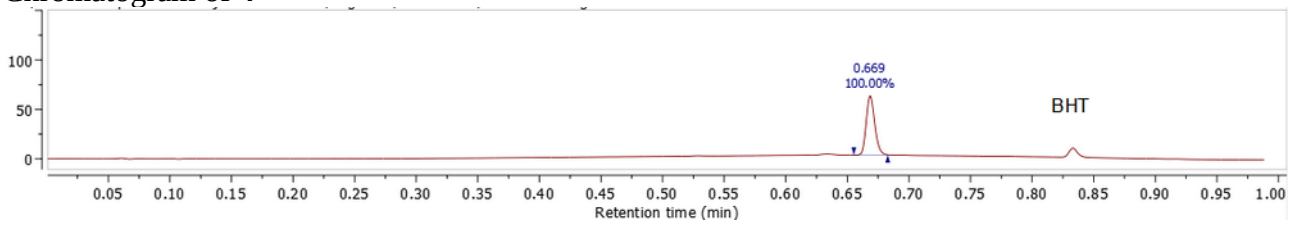
Downloaded from pubs.acs.org/oprdfk/article-supplement/5455873/pdf/op6c00246_si_002/ by guest on 23 October 2026

2.4 Lithiation-protonation of 1,2-Dibromobenzene, 3

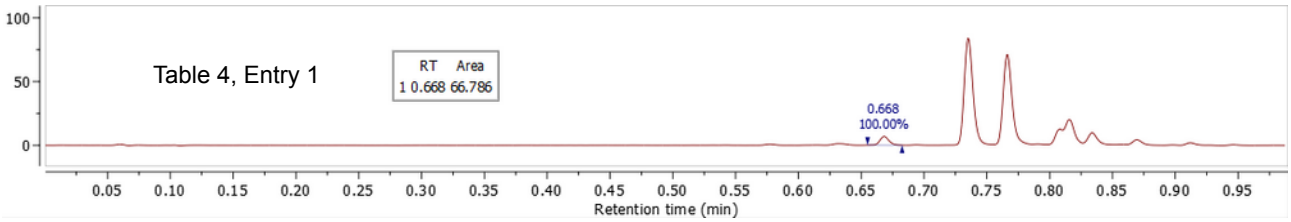
Chromatogram of **3**

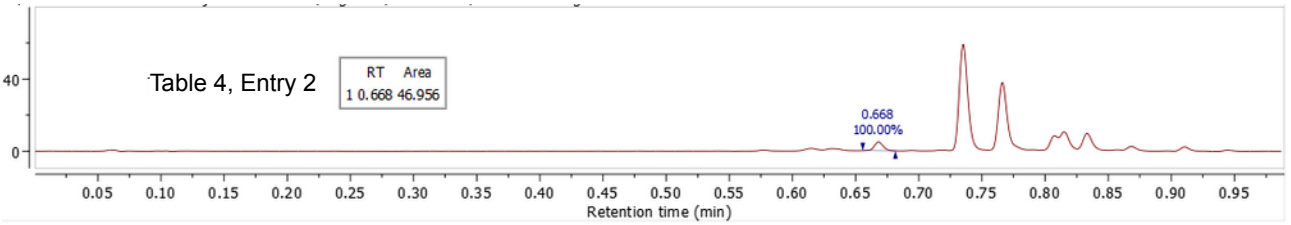


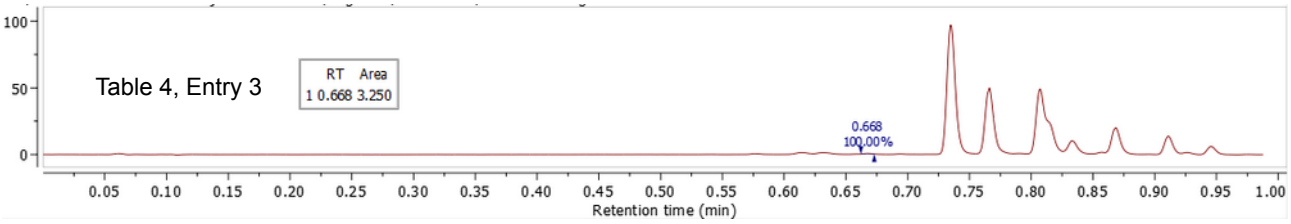
Chromatogram of **4**

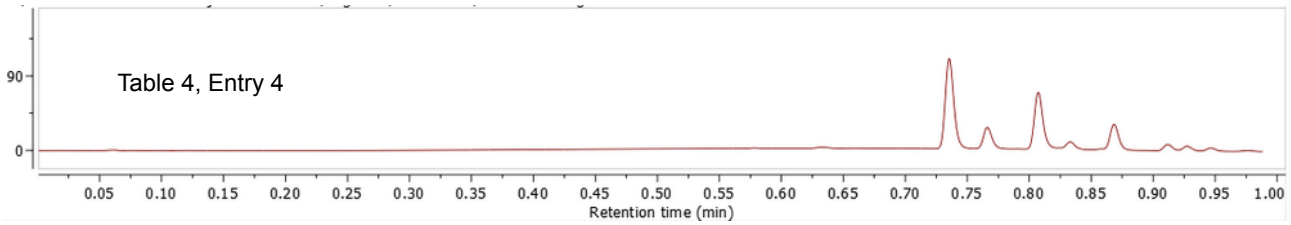


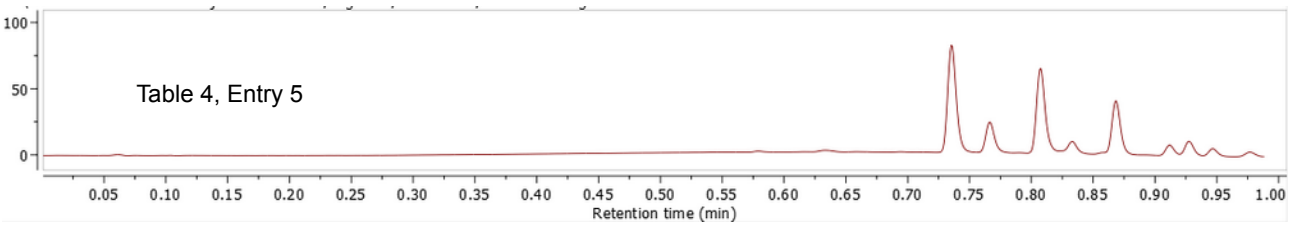
2.4.1 Chromatograms supporting yield calculations for table 4



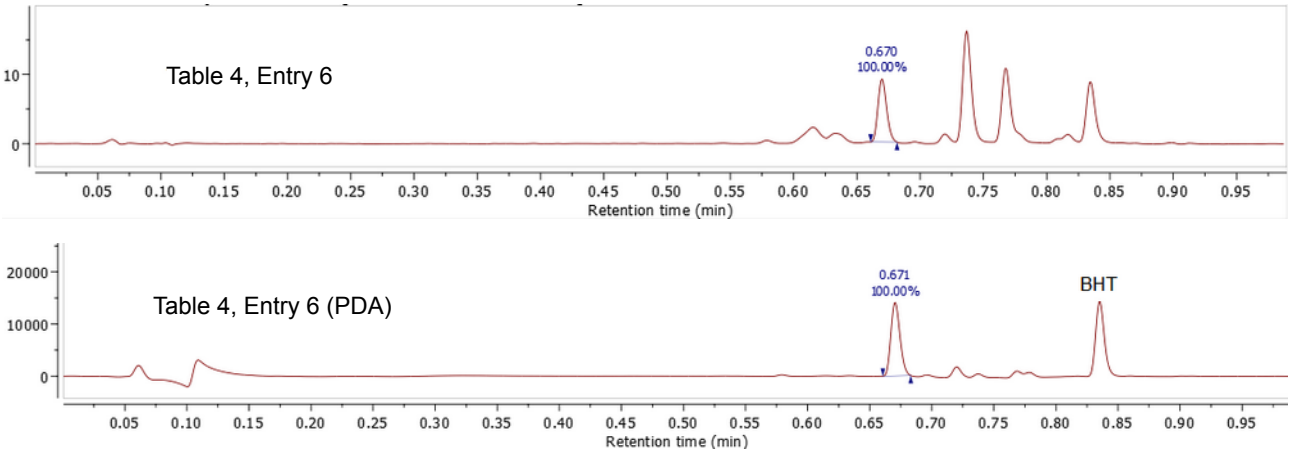




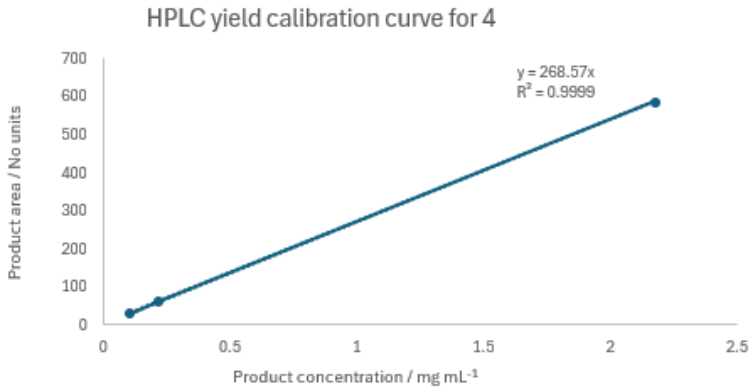




Downloaded from pubs.acs.org/oprd/fk/article-supplement/5455873/pdf/op6c00246_si_002/ by guest on 23 October 2026



2.4.2 Calibration curve for yield determination of 4



2.5 T_{react}-Yield correlations

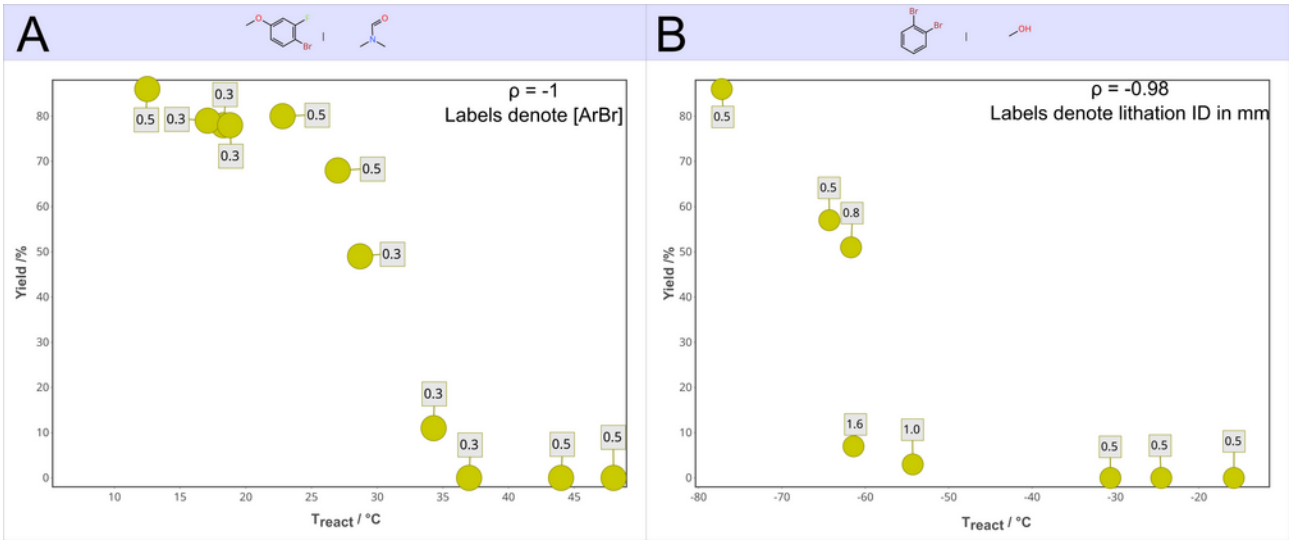


*Figure S6: Yield as a function of T_{react} for: A) the lithitation-formylation of **1** and B) The lithiation-protonation of **3**.*

Downloaded from pubs.acs.org/oprdfk/article-supplement/5455873/pdf/op6c00246_si_002/ by guest on 23 October 2026

2.6 Equipment photos.

2.6.1 Effect of residence time on Δ T

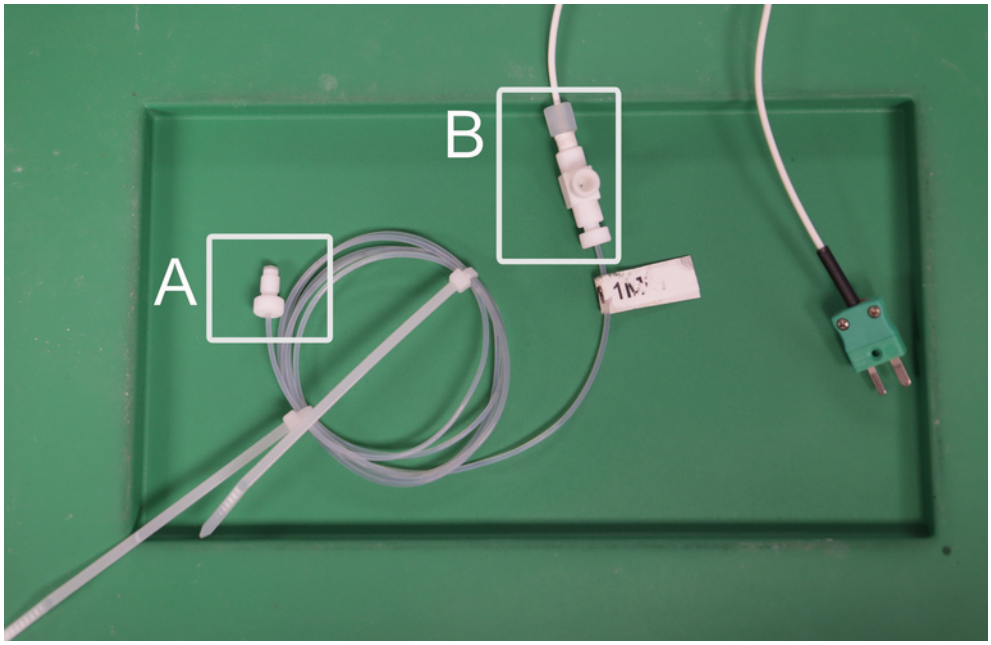


Figure S7: A representative precooling line (ID x OD 1.0 x 1.6 mm) used as part of the work. A) The solvent inlet. B) The inline thermocouple which is connected in a "head-on" configuration. Solvent flows out of the unconnected part of the tee-piece, through an additional piece of tubing.

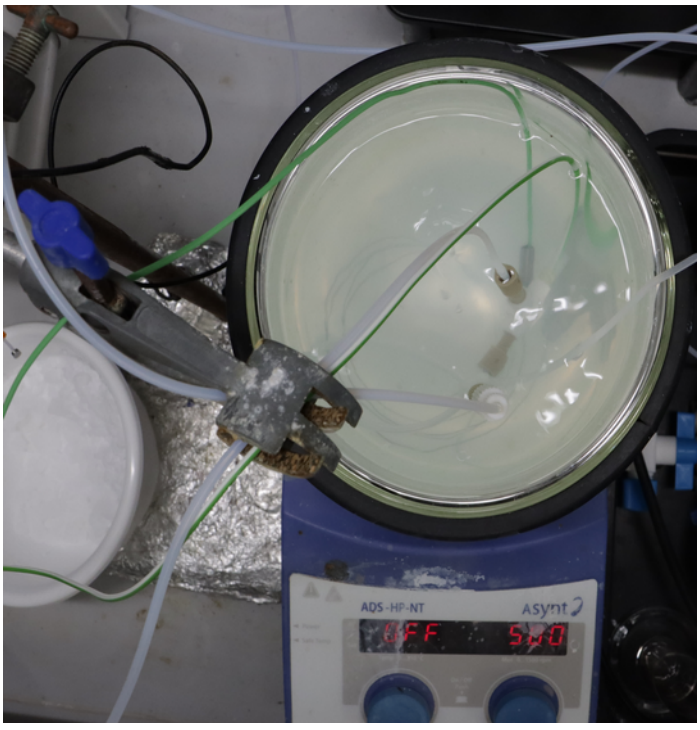


Figure S8: Image of a residence time vs ΔT determination experiment.

Downloaded from pubs.acs.org/oprdfk/article-supplement/5455873/pdf/op6c00246_si_002/ by guest on 23 October 2026

2.6.2 Application to cryogenic flow chemistry: Scope and limitations

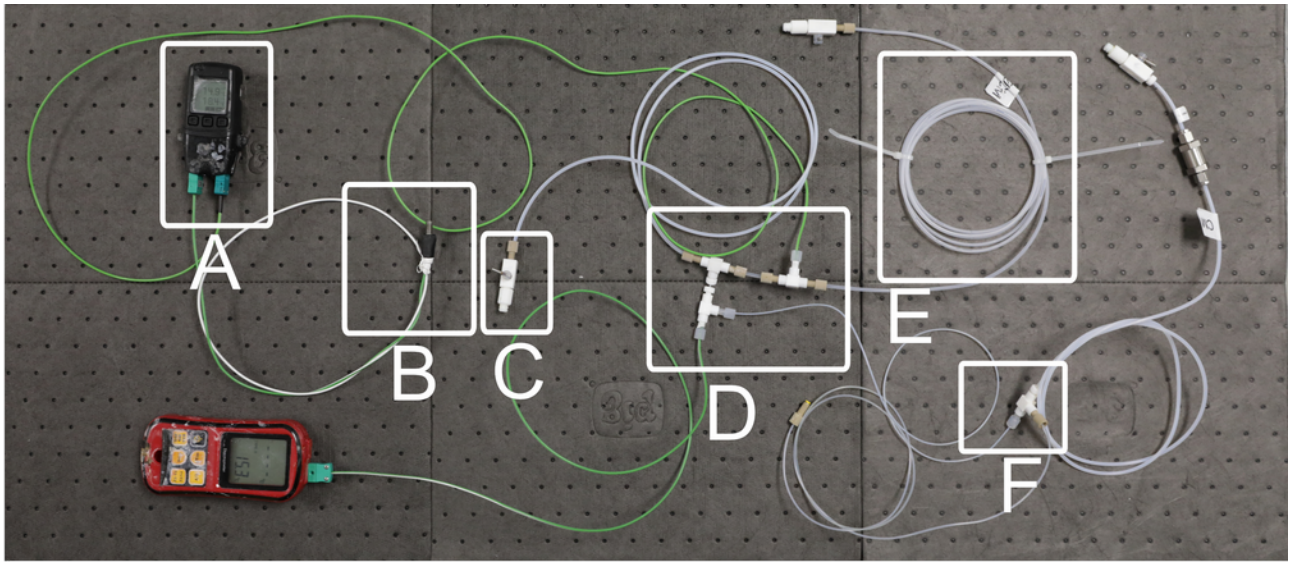


Figure S9: Representative reactor used for lithiation reactions in flow. A) Thermocouple reader. B) Bath temperature (T_{bath}) thermocouple. C) Reactant inlet. D) End of precooling line (T_{inline}), lithiation zone (T_{react}) thermocouples and ArBr/RLi mixing junction (see expansion). E) ArBr precooling line. F) ArLi-Electrophile mixing junction.

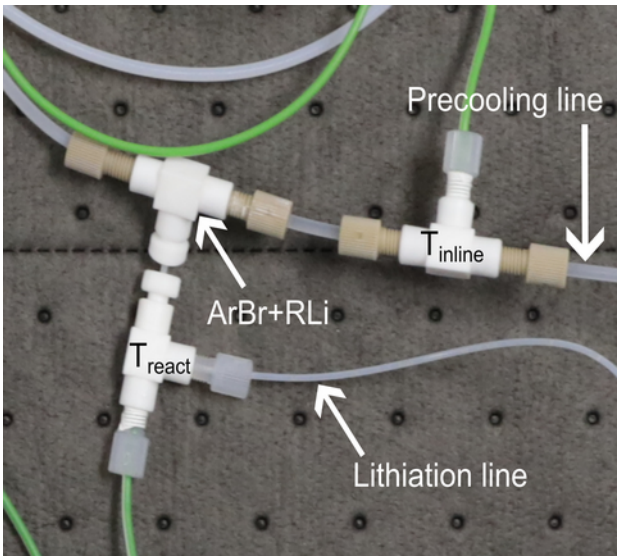


Figure S10: Expansion of the in-line thermocouple configuration in Figure S9.

Downloaded from pubs.acs.org/oprdfk/article-supplement/5455873/pdf/op6c00246_si_002/ by guest on 23 October 2026

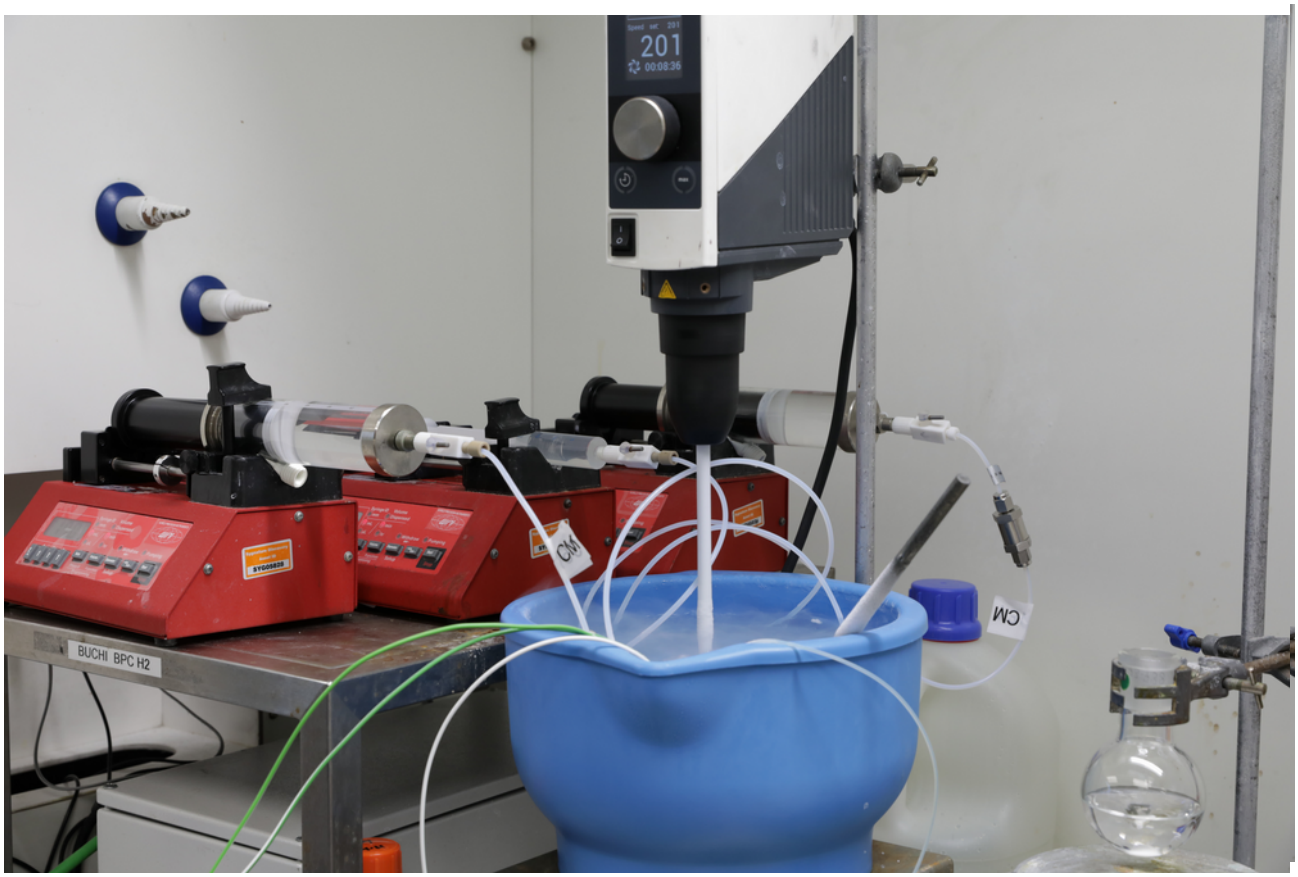


Figure S11: A lithiation experiment in progress.

Downloaded from pubs.acs.org/oprdfk/article-supplement/5455873/pdf/op6c00246_si_002/ by guest on 23 October 2026

3 Source literature for Figure 1

References were randomly selected from Spennacchio[2] and Zhou[3]. Criteria for inclusion were the reporting of precooling loop conditions, typically in the supporting information. This resulted in the identification of 23 original articles and 53 precooling lines (i.e. multiple precooling lines were reported per work). Data were tabulated and parameters such as volume or residence time were calculated through the data available in the references and are available in the raw data package. The references were:

1. Natho, P.; Colella, M.; Andresini, M.; Degennaro, L.; Luisi, R. Taming 3-Oxetanyllithium Using Continuous Flow Technology. Org. Lett. 2024, 26 (15), 3032–3036. https://doi.org/10.1021/acs.orglett.4c00644.
2. Okano, K.; Yamane, Y.; Nagaki, A.; Mori, A. Trapping of Transient Thienyllithiums Generated by Deprotonation of 2,3- or 2,5-Dibromothiophene in a Flow Microreactor. Synlett 2020, 31 (19), 1913–1918. https://doi.org/10.1055/s-0040-1706479.
3. Lee, H.-J.; Kwak, C.; Kim, D.-P.; Kim, H. Continuous-Flow Si–H Functionalizations of Hydrosilanes via Sequential Organolithium Reactions Catalyzed by Potassium Tert-Butoxide. Green Chem. 2021, 23 (3), 1193–1199. https://doi.org/10.1039/D0GC03213A.
4. Harenberg, J. H.; Weidmann, N.; Wiegand, A. J.; Hoefer, C. A.; Annapureddy, R. R.; Knochel, P. (2-Ethylhexyl)Sodium: A Hexane-Soluble Reagent for Br/Na-Exchanges and Directed Metalations in Continuous Flow. Angewandte Chemie International Edition 2021, 60 (26), 14296–14301. https://doi.org/10.1002/anie.202103031.
5. Djukanovic, D.; Heinz, B.; Mandrelli, F.; Mostarda, S.; Filipponi, P.; Martin, B.; Knochel, P. Continuous Flow Acylation of (Hetero)Aryllithiums with Polyfunctional N , N -Dimethylamides and Tetramethylurea in Toluene. Chemistry A European J 2021, 27 (56), 13977–13981. https://doi.org/10.1002/chem.202102805.
6. Harenberg, J. H.; Weidmann, N.; Karaghiosoff, K.; Knochel, P. Continuous Flow Sodiation of Substituted Acrylonitriles, Alkenyl Sulfides and Acrylates. Angewandte Chemie International Edition 2021, 60 (2), 731–735. https://doi.org/10.1002/anie.202012085.
7. Kremsmair, A.; Wilke, H. R.; Harenberg, J. H.; Bissinger, B. R. G.; Simon, M. M.; Alandini, N.; Knochel, P. In Situ Quench Reactions of Enantioenriched Secondary Alkyllithium Reagents in Batch and Continuous Flow Using an I/Li-Exchange. Angewandte Chemie International Edition 2023, 62 , e202214377. https://doi.org/10.1002/anie.202214377.
8. Hafner, A.; Meisenbach, M.; Sedelmeier, J. Flow Chemistry on Multigram Scale: Continuous Synthesis of Boronic Acids within 1 s. Org. Lett. 2016, 18 (15), 3630–3633. https://doi.org/10.1021/acs.orglett.6b01681.

2 Spennacchio, M.; Natho, P.; Andresini, M.; Colella, M. Continuous Flow Generation of Highly Reactive Organometallic Intermediates: A Recent Update. J Flow Chem, 2024. https://doi.org/10.1007/s41981-023-00292-y.

3 Zhou, F.; Zhou, Y.; Duanmu, C.; Li, Y.; Li, J.; Xu, H.; Wang, P.; Zhu, K. Advances in Flow Chemistry for Organolithium-Based Synthesis: A Process Perspective. Molecules 2026, 31 (1), 105. https://doi.org/10.3390/molecules31010105.

Downloaded from pubs.acs.org/oprdfk/article-supplement/5455873/pdf/op6c00246_si_002/ by guest on 23 October 2026

9. Hafner, A.; Mancino, V.; Meisenbach, M.; Schenkel, B.; Sedelmeier, J. Dichloromethyllithium: Synthesis and Application in Continuous Flow Mode. Org. Lett. 2017, 19 (4), 786–789. https://doi.org/10.1021/acs.orglett.6b03753.

10. Ketels, M.; Konrad, D. B.; Karaghiosoff, K.; Trauner, D.; Knochel, P. Selective Lithiation, Magnesiation, and Zincation of Unsymmetrical Azobenzenes Using Continuous Flow. Org. Lett. 2017, 19 (7), 1666–1669. https://doi.org/10.1021/acs.orglett.7b00460.

11. Ketels, M.; Ziegler, D.; Knochel, P. Selective Zincation of 1,2-Dicyanobenzene and Related Benzonitriles in Continuous Flow Using In Situ Trapping Metalations. Synlett 2017, 28 (20), 2817–2822. https://doi.org/10.1055/s-0036-1588837.

12. Colella, M.; Musci, P.; Cannillo, D.; Spennacchio, M.; Aramini, A.; Degennaro, L.; Luisi, R. Development of a Continuous Flow Synthesis of 2-Substituted Azetines and 3-Substituted Azetidines by Using a Common Synthetic Precursor. J. Org. Chem. 2021, 86 (20), 13943–13954. https://doi.org/10.1021/acs.joc.1c01297.

13. Brégent, T.; Ivanova, M. V.; Poisson, T.; Jubault, P.; Legros, J. Continuous-Flow Divergent Lithiation of 2,3-Dihalopyridines: Deprotolithiation versus Halogen Dance. Chemistry – A European Journal 2022, 28 (71), e202202286. https://doi.org/10.1002/chem.202202286.

14. Dunn, A. L.; Leitch, D. C.; Journet, M.; Martin, M.; Tabet, E. A.; Curtis, R.; Williams, G.; Goss, C.; Shaw, T.; O'Hare, B.; Wade, C.; Toczko, M. A.; Liu, P. Selective Continuous Flow Iodination Guided by Direct Spectroscopic Observation of Equilibrating Aryl Lithium Regioisomers. Organometallics. 2019, 38 (1): 129–137

15. Shan, C.; Xu, J.; Cao, L.; Liang, C.; Cheng, R.; Yao, X.; Sun, M.; Ye, J. Rapid Synthesis of α-Chiral Piperidines via a Highly Diastereoselective Continuous Flow Protocol. Org. Lett. (2022) 24 (17): 3205–3210.

16. Newby, J. A.; Blaylock, D. W.; Witt, P. M.; Pastre, J. C.; Zacharova, M. K.; Ley, S. V.; Browne, D. L. Design and Application of a Low-Temperature Continuous Flow Chemistry Platform. Org. Process Res. Dev. 2014, 18 (10), 1211–1220. https://doi.org/10.1021/op500213j.

17. von Keutz, T.; Cantillo, D.; Kappe, C. O. Continuous Flow Synthesis of Terminal Epoxides from Ketones Using in Situ Generated Bromomethyl Lithium. Org. Lett. 2019, 21 (24), 10094–10098. https://doi.org/10.1021/acs.orglett.9b04072.

18. Nagaki, A.; Takahashi, Y.; Yoshida, J. Generation and Reaction of Carbamoyl Anions in Flow: Applications in the Three-Component Synthesis of Functionalized α-Ketoamides. Angewandte Chemie 2016, 128 (17), 5413–5417. https://doi.org/10.1002/ange.201601386.

19. Ichinari, D.; Ashikari, Y.; Mandai, K.; Aizawa, Y.; Yoshida, J.; Nagaki, A. A Novel Approach to Functionalization of Aryl Azides through the Generation and Reaction of Organolithium Species Bearing Masked Azides in Flow Microreactors. Angewandte Chemie International Edition 2020, 59 (4), 1567–1571. https://doi.org/10.1002/anie.201912419.

20. Lee, H.-J.; Torii, D.; Jeon, Y.; Yoshida, J.; Kim, H. Integrated Synthesis Using Isothiocyanate-Substituted Aryllithiums by Flow Chemistry. Synlett 2020, 31 (19), 1899–1902. https://doi.org/10.1055/s-0040-1707251.

Downloaded from pubs.acs.org/oprdfk/article-supplement/5455873/pdf/op6c00246_si_002/ by guest on 23 October 2026

21. Kohyama, A.; Namioka, M.; Naka, H.; Ashikari, Y.; Nagaki, A.; Takikawa, H.; Yamaoka, Y.; Takasu, K. Continuous Flow Synthesis of Cyclobutenes via Lithium Ynolates. Green Chem. 2025, 27 (10), 2760–2765. https://doi.org/10.1039/D4GC05102E.

22. Thaisrivongs, D. A.; Naber, J. R.; McMullen, J. P. Using Flow To Outpace Fast Proton Transfer in an Organometallic Reaction for the Manufacture of Verubecestat (MK-8931). Org. Process Res. Dev. 2016, 20 (11), 1997–2004. https://doi.org/10.1021/acs.oprd.6b00247.

23. Degennaro, L.; Maggiulli, D.; Carlucci, C.; Fanelli, F.; Romanazzi, G.; Luisi, R. A Direct and Sustainable Synthesis of Tertiary Butyl Esters Enabled by Flow Microreactors. Chem. Commun. 2016, 52 (61), 9554–9557. https://doi.org/10.1039/C6CC04588J.

Downloaded from pubs.acs.org/oprdfk/article-supplement/5455873/pdf/op6c00246_si_002/ by guest on 23 October 2026